ACS APPLIED MATERIALS & INTERFACES

Research Article

www.acsami.org

pH-Guided Self-Assembly of Copper Nanoclusters with Aggregation-Induced Emission

Xuxian Su and Jinbin Liu*

Key Laboratory of Functional Molecular Engineering of Guangdong Province, School of Chemistry and Chemical Engineering, South China University of Technology, Guangzhou 510640, China

Supporting Information

ABSTRACT: We here report a facile pH-guided strategy for the fabrication of water-soluble protein/copper nanoclusters (CuNCs) hybrid nanostructures with stable and bright luminescence resulted from aggregation-induced emission. Using L-cysteine as both the reducing and capping agents, the synthesized CuNCs showed a good reversible pH-responsive aggregation and dispersion in the solution. The CuNCs formed insoluble macroscopic aggregates with stable red-colored emission (620 nm) at pH 3.0 but became soluble with weak luminescence at pH <1.5 or pH >4.0. The highly reversible pH-responsive properties of the CuNCs made it feasible to achieve water-soluble protein/CuNCs hybrid nanostructures in the presence of protein without any external forces (e.g., sonication). The weak luminescent CuNCs were first mixed with protein under neutral condition (e.g., pH 7.0), followed by tuning of the pH to acidic conditions (e.g., pH 3.0) to form luminescent protein/CuNCs hybrid nanostructures, the sizes of which were much smaller than those of the protein-free macroscopic CuNC aggregates. This strategy was easily applicable to other dispersing agents (e.g., glucose oxidase), opening a new pathway for the construction of many other smart water-soluble luminescent biomolecule/nanocluster hybrid nanostructures with various applications.

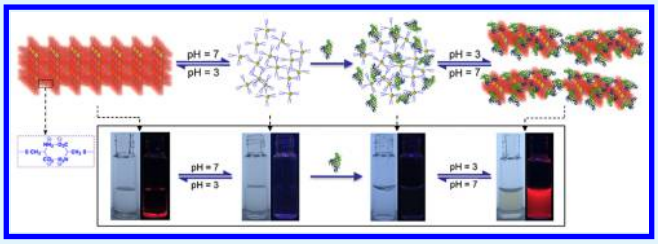

KEYWORDS: *self-assembly, copper nanocluster, noncovalent decoration, water-soluble, hybrid nanostructure*

INTRODUCTION

The molecular metal nanoparticles including few-atom metal nanoclusters (NCs) and few-nanometer nanoparticles (NPs) with molecule-like properties are promising luminescent probes for recognition of chemical species and bioimaging because of their unique optical properties and good biocompatibility.[1−10] Among all of the luminescent metals, the copper-based nanomaterials are of immense interest because of the earth-abundant and relatively low cost of copper.[11−13] Recently, various synthetic strategies of CuNCs have been reported using different molecular templates such as protein,[14,15] DNA,[16,17] and small thiolated ligands.[18−21] However, it is still difficult to directly achieve stable and bright emissive CuNCs, and most of the methods were inclined to form unstable or large particles because of the easy surface oxidation of copper upon exposure to air.[22] Therefore, the development of green and facile synthesis of chemically stable luminescent CuNCs in aqueous solution remains a challenge.

The strategy of aggregation-induced emission (AIE) has recently been exploited to make weak-emitting CuNCs highly luminescent,[23,24] resulting from the surface ligand coupling and cuprophilic interactions to activate the restriction of intramolecular rotation or vibration,[25−28] which provides a promising methodology for the design of highly luminescent CuNCs. For example, CuNCs prepared with glutathione in mixed solvents of ethanol and water exhibited quantum yields (QYs) up to 6.6% after the ethanol fraction was increased more than 80%.[29] By taking the advantage of noncovalent interactions from the surface ligands of the CuNCs, the pH was also found to enhance aggregation to induce the emission of CuNCs coated by D-penicillamine with a high QY of 16.6%.[23] Besides enhancement of the luminescence performance, the alternation of the CuNCs connection fashion after the assembly based on the AIE strategy would greatly extend potential applications of the CuNCs.[30,31] However, unlike the monodispersed individual CuNCs, the AIE-based strategy often requires the CuNCs to form large aggregates with poor solubility and low stability in the aqueous suspension,[32] which would hamper applications that require nanomaterials with good solubility.[33−37]

Herein, we report a facile pH-guided mild strategy to fabricate water-soluble protein-conjugated CuNC hybrid nanostructures with stable and bright emission. Using L-cysteine as a model ligand, the CuNCs were synthesized to form macroscopic insoluble aggregates, resulting in a strong AIE behavior with emission at 620 nm at pH 3.0, whereas the CuNCs became soluble at pH <1.5 or >4.0 and the emission of CuNCs became weak or even disappeared. The pH-responsive emission and aggregation of the CuNCs were highly reversible, which offered us a great opportunity to achieve well-dispersed

Received: October 31, 2016
Accepted: January 9, 2017
Published: January 9, 2017

DOI: 10.1021/acsami.6b13914
ACS Appl. Mater. Interfaces 2017, 9, 3902−3910

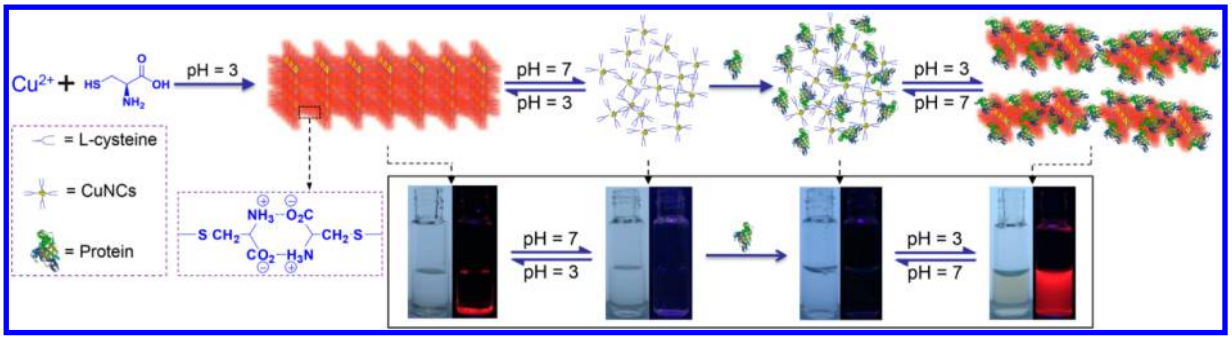

Figure 1. Schematic diagram of the pH-guided strategy in the fabrication of water-soluble protein/CuNCs hybrid nanostructures.

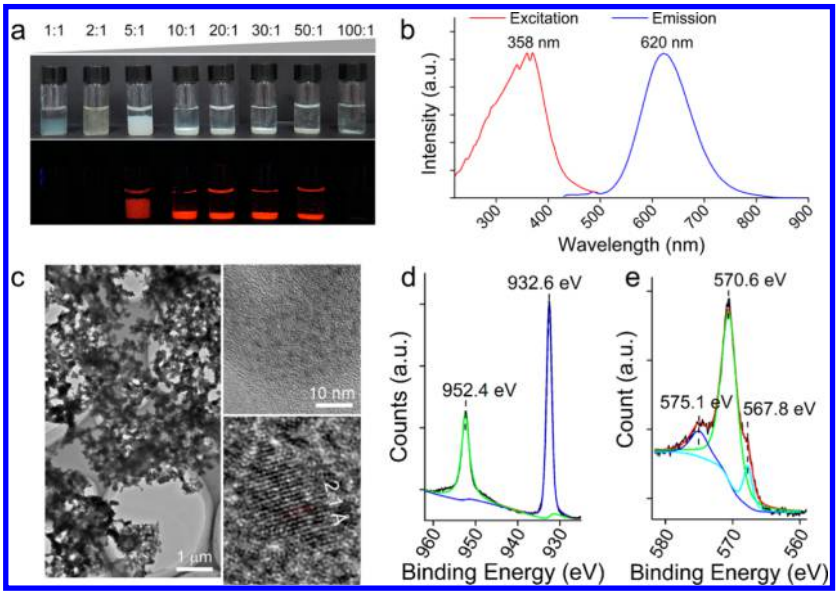

Figure 2. Characterization of the synthesized CuNC aggregates. (a) Photographs of the CuNC aggregates synthesized at different molar ratios of cysteine to Cu^{2+} (cysteine/Cu^{2+}) after aging overnight at room temperature, and the pictures were taken under room light (upper panel) and 365 nm UV light (lower panel). (b) Excitation and emission spectra of CuNC aggregates. (c) Typical TEM images of the CuNC aggregates at different magnifications (pH 3.0). (d) XPS of the Cu 2p spectrum in CuNC aggregates with no satellite peaks observed, evidencing the absence of copper(II) species. (e) Peak-fitted copper LMM Auger spectrum for the CuNC aggregates.

luminescent CuNCs via protein noncovalent decoration through pH control. The soluble weak luminescent CuNCs were first mixed with BSA under neutral conditions (e.g., pH 7.0), followed by tuning of the pH of solution to 3.0 to form the water-soluble luminescent protein/CuNCs hybrid nanostructures (Figure 1). Interestingly, the sizes of the BSA/CuNCs hybrid nanostructures became much smaller than those of the protein-free macroscopic aggregate but preserved comparable luminescence properties and QYs (CuNC aggregates, 5.4% in solid and 1.9% in suspension; BSA/CuNCs, 6.3% in solid and 2.1% in aqueous solution). This pH-guided strategy was highly extendable to glucose oxidase (GOx) in the formation of GOx/CuNCs hybrid nanostructures, which was demonstrated as a powerful optical nanoplatform for glucose sensing in solution. This pH-guided strategy is distinct from the conventional methods (e.g., sonication-[38] or solvent-induced aggregation[10]) in the fabrication of optical water-soluble nanostructures with AIE behavior, which is excellent at overcoming the incompatibilities between the solubility and AIE and expected to design more bionanoplatforms in the applications of biosensing, imaging, and nanomedicine.

EXPERIMENTAL SECTION

Synthesis of the CuNCs. An L-cysteine aqueous solution (4.0 mL, 5−500 mM) was mixed with 20 μL of a 1 M $CuCl_2$ aqueous solution at mole ratios from 1:1 to 1:100 for cysteine to $CuCl_2$ at room temperature. The solution quickly turned from nearly violet to pale white and formed a precipitate at the bottom of the solution. Under 365 nm UV-light radiation, a bright-red emission of aggregates was clearly visible, indicating the formation of luminescent CuNC aggregates.

pH-Guided Self-Assembly of Protein/CuNCs Hybrid Nanostructures. The protein/CuNCs hybrid nanostructures were prepared by mixing CuNC aggregates with an excess amount of protein (BSA or GOx). Typically, the synthesized CuNC aggregates were first dissolved in solution with weak luminescence at pH 7.0, followed by the addition of the BSA solution at different concentrations (final BSA concentrations of 1.0, 2.0, 5.0, and 10.0 mg/mL or a final GOx concentration of 10 mg/mL). The above mixture was then mixed thoroughly and incubated at room temperature for 10 min before the pH of the above solution was adjusted back to 3.0. The red emission of the solution was clearly visible under 365 nm UV light, and no precipitate was observed in the solution, indicating formation of the water-soluble protein/CuNCs hybrid nanostructures. The free protein was purified by a Sephadex G25 column, and the red-emissive protein/CuNCs hybrid nanostructures were collected under 365 nm UV light.

DOI: 10.1021/acsami.6b13914
ACS Appl. Mater. Interfaces 2017, 9, 3902−3910

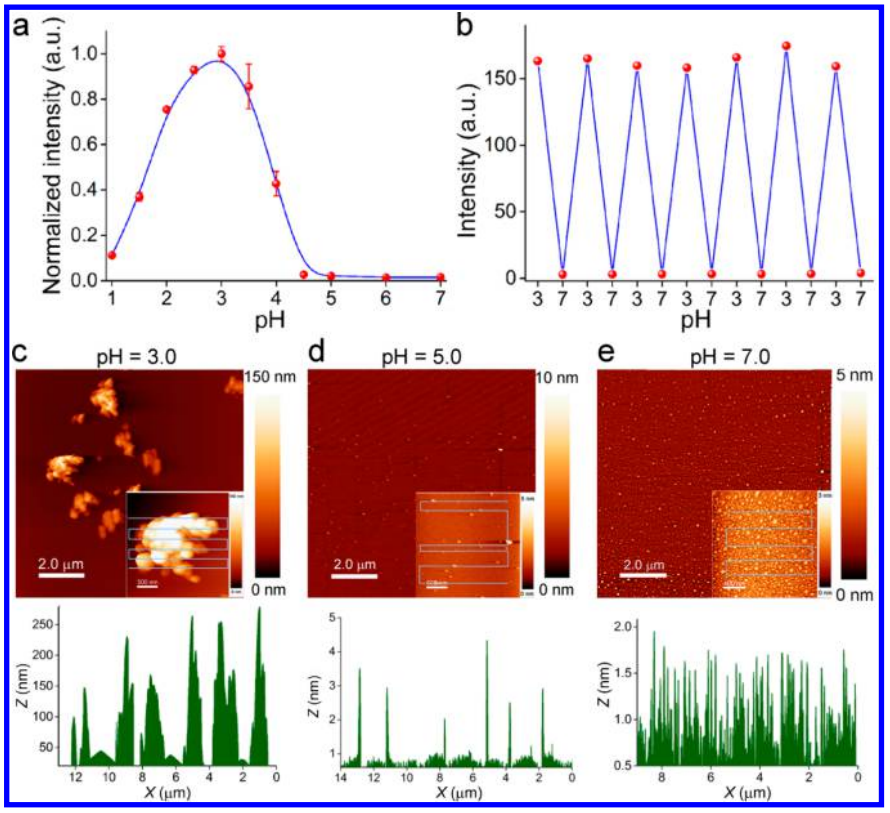

Figure 3. pH-responsive properties of the synthesized CuNCs. (a) Plot of the emission intensity of the CuNCs in a PBS buffer over different pH values. (b) Reversibility of the pH-dependent emission of the CuNCs between pH 3.0 and 7.0. (c–e) AFM image (upper panel) and the corresponding height profile (lower panel) of the CuNCs at different pH values (pH 3.0, 5.0, and 7.0). Insets: Corresponding magnified AFM images for the height analysis.

Detection of Glucose. Different concentrations of glucose stock solutions were freshly prepared before use. To a 1.5 mL centrifuge tube was added 40 μL of a GOx/CuNCs solution, 40 μL of a glycine/HCl buffer (pH 3.0), and 4.0 μL of glucose solutions (final concentrations: 0–100 μM), and then the resulting solution was diluted to 400 μL in total volume with water. The mixture was mixed thoroughly and incubated for 40 min at room temperature before the luminescence measurements. The glucose concentration-dependent luminescence quenching efficiency (I/I_0 %, where I_0 and I represent the luminescence intensities of GOx/CuNCs before and after the incubation of glucose, respectively) was then obtained, and a calibration curve was established. For the selectivity test, the other carbohydrates and other metal ions were used as interference substances (100 μM) including D-fructose, maltose, α-laltose, cucrose, L-ascorbic acid (Vc), K^+, Na^+, Ca^{2+}, Zn^{2+}, and Fe^{3+}.

RESULTS AND DISCUSSION

Synthesis and Characterization of the CuNCs. The macroscopic red-emitting CuNC aggregates were synthesized by mixing L-cysteine with $CuCl_2$ at mole ratios from 1:1 to 100:1 in solution at room temperature. Neither a ratio smaller than 5:1 nor more than 100:1 could generate red-emitting CuNC aggregates (Figure 2a). The CuNC aggregates exhibited strong emission with a maximum at 620 nm (λ_{ex} = 358 nm). The large Stokes shift (262 nm; Figure 2b) indicated that the emission of CuNC aggregates should be related to the coordination of copper(I) with the capping ligand cysteine, induced from charge transfer through ligand-to-metal charge transfer (LMCT) and/or ligand-to-metal–metal charge transfer (LMMCT).[39] We also checked the emission spectra of CuNC aggregates after washing with water three times to remove the random hybrid cluster that might be generated in the aggregated system (Figure S1), and the emission spectra of CuNC aggregates did not change after normalization although the values of the emission intensity decreased because of dissolution of the CuNCs during the water-washing process. The results demonstrated that the broad emission of CuNCs was a typical molecular luminescence instead of the emission caused from the randomly generated hybrid cluster in our system.[23] The absolute QYs of the macroscopic CuNC aggregates were measured to be 5.4% in solid and 1.9% in suspension at pH 3.0. The emission of synthesized CuNC aggregates was highly stable for more than 2 weeks at room temperature and even longer than 2 months when stored in a refrigerator at 4 °C. The disappearance of the –SH stretching mode at 2550 cm^{-1} suggested that L-cysteine molecules bind with copper through Cu–S bonding (Figure S2). The morphology of the synthesized CuNC aggregates was characterized with transmission electron microscopy (TEM) and scanning electron microscope (SEM). The aggregated lamellar structures of the CuNCs were clearly visible from both the TEM (Figure 2c) and SEM (Figure S3) images, evidencing the AIE behavior of the red-emitting CuNC aggregates. The lattice distance of 2.1 Å of the CuNC aggregates corresponded to the (111) plane of cubic-structured copper.[19] A powder X-ray diffraction (XRD) experiment was also performed to determine the structure and composition of CuNC aggregates (Figure S4). Characteristic diffraction peaks in the 2θ range from 30° to 80° were usually observed from the bulk CuNPs.[40] The CuNC aggregates did not possess all of the characteristic diffraction peaks of bulk CuNPs, indicating the small sizes of the CuNCs in the aggregates.[41]

DOI: 10.1021/acsami.6b13914
ACS Appl. Mater. Interfaces 2017, 9, 3902–3910

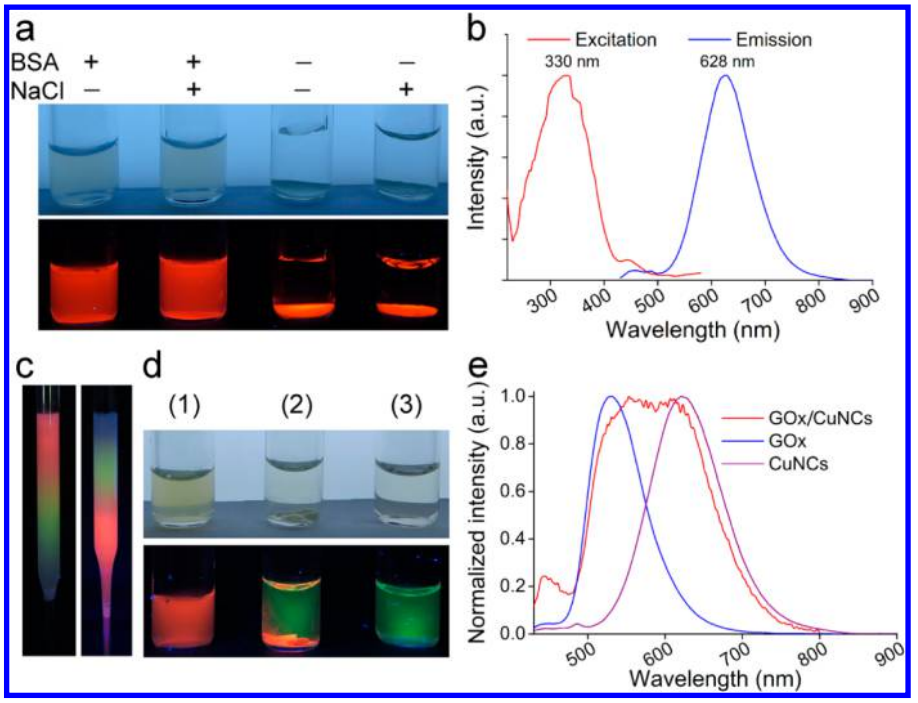

Figure 4. Self-assembly of the water-soluble protein/CuNCs hybrid nanostructures. (a) Stability test of the BSA/CuNCs hybrid nanostructures after centrifugation at 2000*g* for 1 min in the presence of 0.1 M NaCl. The photographs were taken under room light (upper panel) and 365 nm UV light (lower panel). (b) Excitation and emission spectra of BSA/CuNCs hybrid nanostructures in aqueous solution. (c) Purification of the GOx/CuNCs hybrid nanostructures with a Sephadex G25 column (pH 3.0). The photographs of the Sephadex G25 column loadings with samples of a mixture of GOx and CuNC aggregates (left) and GOx/CuNCs hybrid nanostructures (right) were taken under 365 nm UV light. (d) Photographs of the purified GOx/CuNCs hybrid nanostructures, a mixture of GOx and CuNC aggregates, and pure GOx after centrifugation (pH 3.0) at 2000*g* for 1 min taken under room light (upper panel) and 365 nm UV light (lower panel). (e) Emission spectra of a purified GOx/CuNCs hybrid nanostructure, GOx, and CuNCs.

The valence states of the copper in the CuNC aggregates were investigated by X-ray photoelectron spectroscopy (XPS, Figure 2d,e). The Cu 2p spectrum exhibited two binding energy peaks at 932.6 and 952.4 eV with an area ratio of 2:1, which could be assigned to the Cu $2p_{3/2}$ and Cu $2p_{1/2}$ signals, respectively, which originated from the copper(I) or copper(0) species. The absence of additional shakeup satellite peaks from 938 to 946 eV indicated the absence of copper(II) species in the aggregated CuNCs.[42] The emergence of a strong peak at 570.6 eV and a small peak at 567.8 eV in the X-ray excited Cu LMM Auger spectrum unambiguously confirmed that the species of copper in the aggregated CuNCs was copper(I) mixed with a small ratio of copper(0) species [copper(I)/copper(0) molar ratio of 1:0.11].[43,44] The high ratio of copper(I) species in the CuNC aggregates would facilitate the copper(I)−copper(I) cuprophilic interaction between the CuNCs in the solution.[29] The XPS results were consistent with the mild reduction environment created by the weak reducing agent cysteine. To study whether copper species affect the luminescence of CuNC aggregates, we used a typical reducing agent, $NaBH_4$, to reduce CuNC aggregates (Figure S5), and the results showed that the luminescence of CuNC aggregates quenched significantly after a reduction of the copper(I) species; even the CuNCs still aggregated at pH 3.0, demonstrating that the copper(I) species played an importance role in the emission of CuNC aggregates.

pH-Responsive Study of the CuNCs. The pH-dependent AIE behavior of the synthesized CuNCs was investigated by adjusting the pH of the suspension, followed by luminescence, UV−vis spectroscopy, and morphology characterizations. The luminescence and morphology of CuNCs were highly pH-dependent from pH 1.0 to 7.0 (Figures 3a and S6). The CuNCs showed a strong emission at pH 3.0 in the aggregate state, but the emission decreased significantly with gradual dissolution of the CuNC aggregates in the solution after the pH increased from 3.0 to 7.0 (or decreased from 3.0 to 1.0), further demonstrating the AIE behavior of the CuNC aggregates resulting from strong hydrogen bonding between the carboxyl and amino groups of the cysteine ligands on the CuNC surface[23,32,45−47] and strong cuprophilic interaction at acidic conditions.[48,49] We also applied UV−vis spectroscopy to study the CuNCs at different pH values (Figure S7). The UV−vis absorption spectral peak of the CuNCs exhibited a red shift from 260 to 275 nm when the pH changed from 7.0 to 3.0, and the intensity of the absorption peak at 275 nm decreased after pH <3.0, which might be attributed to the slight change of the LMCT transition.[50] The subtle variation of the CuNC aggregates and disordered monodispersed CuNCs mainly involves the cysteine interactions on the surface CuNCs and the copper(I) to copper(I) cuprophilic interaction. First, the enhanced cuprophilic interactions facilitate the radiative pathway from the excited-state relaxation dynamics. Second, the restriction of intramolecular vibration and rotation of the coating ligand cysteine reduce the nonradiative relaxation of the excited states. Thus, the luminescence of CuNCs was greatly enhanced after the formation of aggregates at pH 3.0. To further verify this deduction, we added different amounts of ethanol to induce the aggregation of CuNCs, and the CuNCs could still emit efficiently even at pH 5.0 (Figure S8). The highly reversible pH response in both luminescence (Figure

DOI: 10.1021/acsami.6b13914
ACS Appl. Mater. Interfaces 2017, 9, 3902−3910

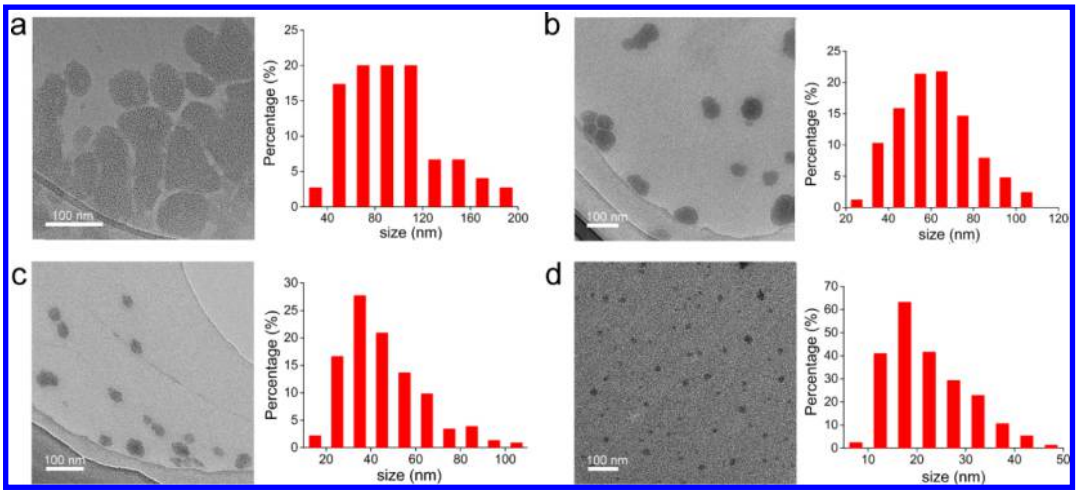

Figure 5. Morphology of the protein/CuNCs hybrid nanostructures. TEM images (left panel) and size distribution (right panel) of the BSA/CuNCs hybrid nanostructures assembled with different concentrations of BSA (a–d: 1.0, 2.0, 5.0, and 10 mg/mL). The average sizes of the BSA/CuNCs were calculated to be 85, 60, 45, and 20 nm, respectively.

3b) and UV–vis absorption (Figure S9) suggested that the synthesized CuNCs were highly stable. It should be noted that the CuNC aggregates after $NaBH_4$ reduction still possessed a reversible pH response ability (Figure S10), but the luminescence of CuNC aggragates completely disappeared, further demonstrating that the emission of the aggregates was induced from the charge transfer through LMCT and/or LMMCT.[30]

As revealed from the atomic force microscopy (AFM) images of the CuNCs at different pH values (Figure 3c–e). The heights of the CuNCs decreased from more than 200 nm to ~1.0 nm with the pH changed from 3.0 to 7.0, indicating that the CuNCs transformed from aggregation to the monodispersed state because of the weaker hydrogen binding and cuprophilic interaction between the CuNCs.[49] In addition, the structures of the CuNCs were also pH-reverisible (Figure S11), which were consistent with the above optical spectral studies. Restricted by the resolution, the tiny CuNCs could not be observed by TEM. The weak luminescent CuNCs at pH 7.0 in the monodispersed state was also analyzed by matrix-assisted laser desorption/ionization time-of-flight mass spectrometry. The characteristic signature of the CuNCs with the highest m/z peak was assigned to $[Cu_8L_6 - H + 2Na]^+$ ($L = C_3H_6NO_2S$) and confirmed from the isotopic mass distribution of copper (Figure S12). The result was also consistent with the element analysis results ($n_{Cu}/n_{cysteine}$ = 1.32; see the details in the Supporting Information).

pH-Guided Self-Assembly of the Water-Soluble Protein/CuNCs Hybrid Nanostructures. The pH-responsive properties of the CuNC aggregates made it feasible to fabricate water-soluble hybrid nanostructures using proteins (e.g., BSA). The proteins with the hydrophobic and hydrophilic patches on their surfaces make them highly adhesive to the surfaces of the nanomaterials.[51] We expected that a protein could have strong absorption ability with CuNCs to form water-soluble hybrid nanostructures. This process started with the addition of an excess amount of BSA to the solution of CuNCs that were water-soluble at pH 7.0. This noncovalent binding of BSA with CuNCs was allowed to take place within 10 min at room temperature before the pH was adjusted back to 3.0, which induced the formation of water-soluble luminescent protein/CuNCs hybrid nanostructures. The hybrid nanostructures showed an obviously red emission and stable dispersion in solution even in the presence of 0.1 M NaCl at pH 3.0 after centrifugation at 2000g (Figure 4a), in sharp contrast to the protein-free macroscopic CuNC aggregates, indicating the successful self-assembly of CuNCs with BSA. Sonication is a commonly used method to disperse insoluble materials or prepare luminescent nanomaterials with AIE,[38,52] and it was very interesting to note that the BSA/CuNCs hybrid nanostructures prepared from the mild pH-guided strategy were much more stable than those made from the sonication-aided dispersion method (Figure S13).

The unconjugated BSA could be removed through a Sephadex G25 column because of the different migration rates between the free BSA and the BSA/CuNCs hybrid nanostructures. As a control experiment, the protein-free CuNC aggregates or the mixture of CuNC aggregates and protein could not pass through the Sephadex G25 column and were trapped on top of the Sephadex G25 column because of their bulky sizes (Figure S14). Although the BSA/CuNCs hybrid nanostructures were highly soluble in the solution, the BSA/CuNCs still showed similar luminescence spectra compared to those of the CuNC aggregates (Figure 4b). The absolute QYs of hybrid nanostructures were 6.3% in the solid state and 2.1% in an aqueous solution, which were comparable to those of the macroscopic CuNC aggregates.

To explore the generality of the assembly strategy and further biological applications, we also used an enzyme (GOx) to perform this assembly process. The free GOx migrated more slowly than the GOx/CuNCs hybrid nanostructures and was clearly visible in the Sephadex G25 column under 365 nm UV light because of the strong autofluorescence of GOx (Figure 4c,d). The GOx/CuNCs hybrid nanostructures showed both the emissions of GOx and CuNCs after removal of the free GOx (Figure 4e), demonstrating the facile self-assembly of GOx with CuNCs, and this assembly process was highly extendable. Interestingly, the emission and absorbance of the BSA/CuNCs hybrid nanostructures showed pH response and reversibility similar to those of the BSA-free CuNC aggregates (Figures S15 and S16).

Characterization of the Protein/CuNCs Hybrid Nanostructures. We then applied TEM and AFM to directly observe the hybrid nanostructures. Figure 5 showed typical

DOI: 10.1021/acsami.6b13914
ACS Appl. Mater. Interfaces 2017, 9, 3902–3910

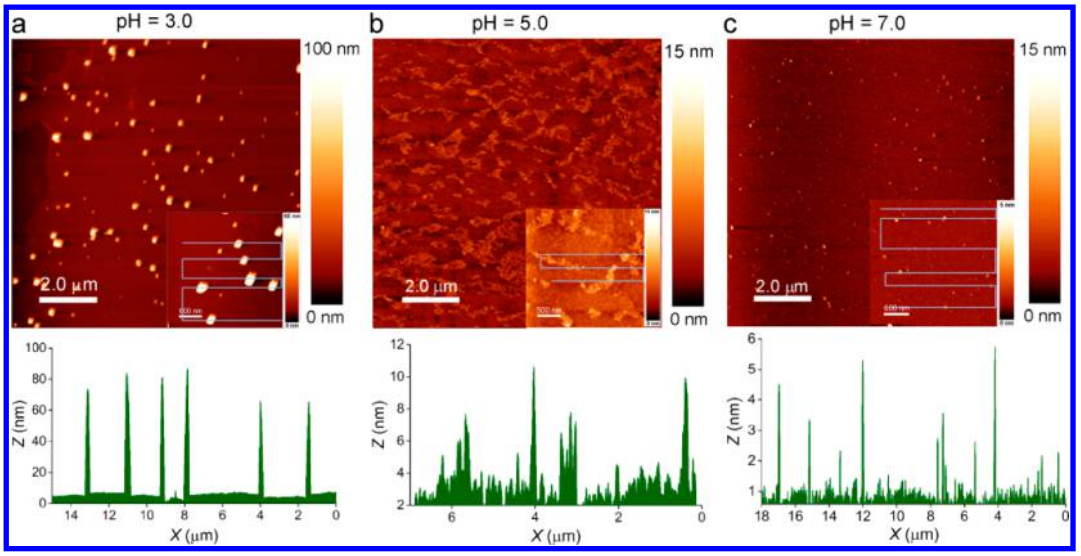

Figure 6. AFM images (upper panel) and the corresponding height profiles (lower panel) of the BSA/CuNCs hybrid nanostructures at different pH values (a–c: 3.0, 5.0, and 7.0). Insets: Corresponding magnified AFM images for the height analysis.

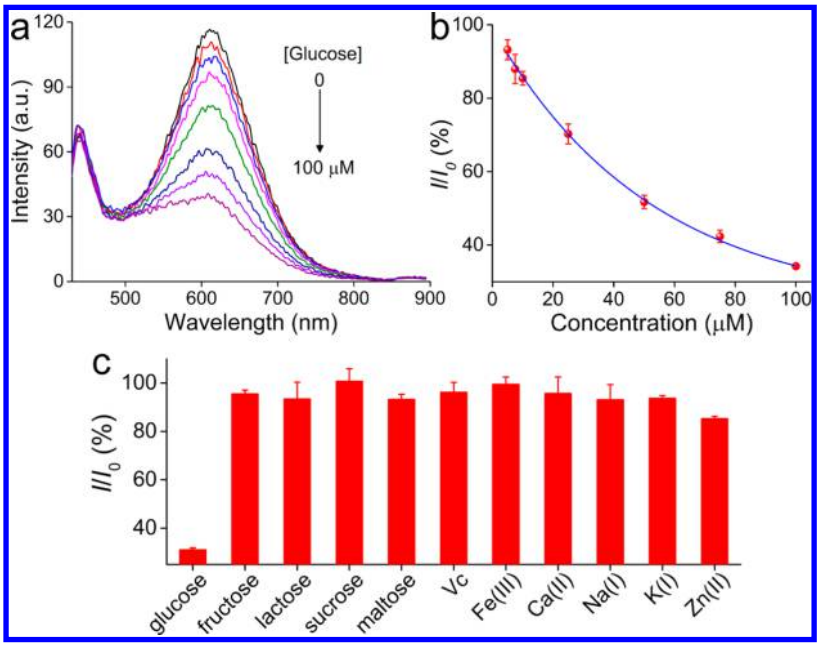

Figure 7. Glucose detection with the GOx/CuNCs hybrid nanostructures. (a) Luminescence spectra of the GOx/CuNCs hybrid nanostructure in the presence of different concentrations of glucose (from top to bottom: 0, 5, 7.5, 10, 25, 50, 75, and 100 μM). (b) Plot of the luminescence quenching efficiency (I/I_0 %) against the glucose concentration. The exponentially fitted equation was $I/I_0 = 76.01 \exp(-c/52.59) + 22.95$ ($R^2 = 0.999$). (c) Selectivity for glucose detection. The quenching efficiencies of glucose were significantly high compared to those of other interfering substances (100 μM), demonstrating the high selectivity for glucose of this proposed method.

TEM images of the BSA/CuNCs hybrid nanostructures assembled with different concentrations of BSA, from which the well-dispersed BSA/CuNCs hybrid nanostructures could be easily observed on the TEM grid. The BSA/CuNCs showed decreased sizes significantly smaller than those of the macroscopic CuNC aggregates. In addition, the size and morphology of BSA/CuNCs could be finely tuned just by changing the BSA concentration. The uniformed morphology of BSA/CuNCs with the sizes in typical Gaussian distributions at high concentrations of BSA indicated that this pH-guided strategy was highly controllable. The assembled BSA/CuNCs hybrid nanostructures could be applicable to many applications such as chemical sensors. Although the sizes of the hybrid nanostructures became much smaller to render them water-soluble and stable in the solution under acidic conditions, the luminescence properties of the hybrid nanostructures were fully preserved compared to those of the protein-free macroscopic CuNC aggregates (Figure S17), which is another important feature of this pH-guided self-assembly strategy.

We also investigated the morphologies of the BSA/CuNCs hybrid nanostructures at different pH values using AFM imaging. The structures of the BSA/CuNCs were also pH-dependent (Figure 6), which formed the hybrid nanostructure at pH 3.0 and disassembled with an increase in the pH to 7.0. The aggregated structures of BSA disassembled from the BSA/CuNCs hybrid nanostructures were clearly visible at pH 5.0

DOI: 10.1021/acsami.6b13914
ACS Appl. Mater. Interfaces 2017, 9, 3902–3910

(isoelectric point of BSA, pH 4.7−5.2). The structures of the BSA/CuNCs were also pH-reversible (Figure S18), which were consistent with the above optical spectral studies. The section analysis from the AFM images of the GOx/CuNCs further demonstrated that this facile pH-induced assembly strategy was highly extendable (Figure S19).

Detection of Glucose. The combination of a biofunctional protein/GOx and the optical nanoprobe/NC in the fabrication of hybrid nanostructures would lead to important analytical applications. Glucose can be oxidized by oxygen (O_2) in the presence of GOx through the reaction glucose + O_2 + $H_2O \xrightarrow{GOx}$ glucose acid + H_2O_2. The generated H_2O_2 would quench the luminescence of CuNCs. Therefore, a facile glucose detection strategy was constructed by the amount of enzymatically generated H_2O_2 based on the GOx/CuNCs hybrid nanostructures. The decrease of the GOx/CuNCs emission intensity responded selectively and was exponentially fitted with increasing concentrations of glucose from 5 to 100 μM (Figure 7). The limit of detection of glucose was 1.5 μM based on the 3δ criterion (Figure S20), which was much lower than that of the normal physiological level of glucose (4.4−6.6 mM).[53] As shown in Table S1, although the sensitivity was not as high as those of the electrochemical sensors, the developed method was more sensitive than most of the reported optical methods for the detection of glucose.[54,55] Therefore, we have achieved a facile, selective, and sensitive optical method for the detection of glucose based on the luminescence quenching of GOx/CuNCs hybrid nanostructures. Because this pH-guided self-assembly process is more extendable than what we investigated above, this self-assembly strategy for the fabrication of luminescent CuNCs hybrid nanostructures could be found in more downstream applications such as bioimaging, biosensing, and drug delivery.

CONCLUSIONS

In summary, we demonstrated a facile method to assemble protein and CuNCs into water-soluble hybrid nanostructures with AIE behavior under mild conditions. The reversible pH-responsive aggregation and dispersion of the cysteine-coated CuNCs made it feasible to fabricate water-soluble luminescent protein/CuNCs hybrid nanostructures. Using a biofunctional protein GOx as an example, we also demonstrated this assembled nanostructure as a powerful analytical platform for glucose detection. In addition, the luminescent hybrid nanostructures were found to exhibit smaller sizes, higher solubility, and better stability but similar luminescence properties compared to those of the protein-free macroscopic CuNC aggregates under acidic conditions (pH 3.0). The size and morphology of BSA/CuNCs could be well tuned by different BSA concentrations. This mild strategy demonstrated here could be easily extended to other types of dispersing agents, which would be a promising new path for the design and fabrication of smart water-soluble luminescent biomolecule/NCs hybrid nanostructures for specific applications.

ASSOCIATED CONTENT

Supporting Information

The Supporting Information is available free of charge on the ACS Publications website at DOI: 10.1021/acsami.6b13914.

Extra experimental details and supplementary data on the characterizations of synthesized CuNCs and protein/CuNCs hybrid nanostructures (PDF)

AUTHOR INFORMATION

Corresponding Author

*E-mail: cejbliu@scut.edu.cn. Tel.: +86-20-22236846.

ORCID

Jinbin Liu: 0000-0002-2046-131X

Notes

The authors declare no competing financial interest.

ACKNOWLEDGMENTS

This work was supported by National Natural Science Foundation of China (Grant 21573078), The 1000 Young Talent Program, Guangdong Natural Science Funds for Distinguished Young Scholar (Grant 2016A030306024), and Fundamental Research Funds for the Central Universities. We thank Qian Lu for her assistance with the TEM characterizations in Figure 5.

REFERENCES

(1) Zheng, J.; Zhou, C.; Yu, M.; Liu, J. Different Sized Luminescent Gold Nanoparticles. *Nanoscale* **2012**, *4* (14), 4073−4083.

(2) Liu, J.; Yu, M.; Zhou, C.; Zheng, J. Renal Clearable Inorganic Nanoparticles: A New Frontier of Bionanotechnology. *Mater. Today* **2013**, *16* (12), 477−486.

(3) Liu, J.; Yu, M.; Ning, X.; Zhou, C.; Yang, S.; Zheng, J. PEGylation and Zwitterionization: Pros and Cons in the Renal Clearance and Tumor Targeting of Near-IR-Emitting Gold Nanoparticles. *Angew. Chem., Int. Ed.* **2013**, *52* (48), 12572−12576.

(4) Liu, J.; Yu, M.; Zhou, C.; Yang, S.; Ning, X.; Zheng, J. Passive Tumor Targeting of Renal-Clearable Luminescent Gold Nanoparticles: Long Tumor Retention and Fast Normal Tissue Clearance. *J. Am. Chem. Soc.* **2013**, *135* (13), 4978−4981.

(5) Liu, J.; Duchesne, P. N.; Yu, M.; Jiang, X.; Ning, X.; Vinluan, R. D., III; Zhang, P.; Zheng, J. Luminescent Gold Nanoparticles with Size-Independent Emission. *Angew. Chem., Int. Ed.* **2016**, *55* (31), 8894−8898.

(6) Tang, Z.; Xu, B.; Wu, B.; Germann, M. W.; Wang, G. Synthesis and Structural Determination of Multidentate 2,3-Dithiol-Stabilized Au Clusters. *J. Am. Chem. Soc.* **2010**, *132* (10), 3367−3374.

(7) Wang, T.; Wang, D.; Padelford, J. W.; Jiang, J.; Wang, G. Near-Infrared Electrogenerated Chemiluminescence from Aqueous Soluble Lipoic Acid Au Nanoclusters. *J. Am. Chem. Soc.* **2016**, *138* (20), 6380−6383.

(8) Wu, Z.; Gayathri, C.; Gil, R. R.; Jin, R. Probing the Structure and Charge State of Glutathione-Capped $Au_{25}(SG)_{18}$ Clusters by NMR and Mass Spectrometry. *J. Am. Chem. Soc.* **2009**, *131* (18), 6535−6542.

(9) Kauffman, D. R.; Alfonso, D.; Matranga, C.; Ohodnicki, P.; Deng, X.; Siva, R. C.; Zeng, C.; Jin, R. Probing Active Site Chemistry with Differently Charged Au_{25}^{q} Nanoclusters (q = − 1, 0, + 1). *Chem. Sci.* **2014**, *5* (8), 3151−3157.

(10) Luo, Z.; Yuan, X.; Yu, Y.; Zhang, Q.; Leong, D. T.; Lee, J. Y.; Xie, J. From Aggregation-Induced Emission of Au(I)-Thiolate Complexes to Ultrabright Au(0)@Au(I)-Thiolate Core-Shell Nanoclusters. *J. Am. Chem. Soc.* **2012**, *134* (40), 16662−16670.

(11) Gawande, M. B.; Goswami, A.; Felpin, F. X.; Asefa, T.; Huang, X.; Silva, R.; Zou, X.; Zboril, R.; Varma, R. S. Cu and Cu-Based Nanoparticles: Synthesis and Applications in Catalysis. *Chem. Rev.* **2016**, *116* (6), 3722−3811.

(12) Zhou, M.; Tian, M.; Li, C. Copper-Based Nanomaterials for Cancer Imaging and Therapy. *Bioconjugate Chem.* **2016**, *27* (5), 1188−1199.

(13) Hu, X.; Liu, T.; Zhuang, Y.; Wang, W.; Li, Y.; Fan, W.; Huang, Y. Recent Advances in the Analytical Applications of Copper Nanoclusters. *TrAC, Trends Anal. Chem.* **2016**, *77*, 66−75.

(14) Goswami, N.; Giri, A.; Bootharaju, M. S.; Xavier, P. L.; Pradeep, T.; Pal, S. K. Copper Quantum Clusters in Protein Matrix: Potential Sensor of Pb^{2+} Ion. *Anal. Chem.* **2011**, *83* (24), 9676−9680.
(15) Wang, C.; Wang, C.; Xu, L.; Cheng, H.; Lin, Q.; Zhang, C. Protein-Directed Synthesis of pH-Responsive Red Fluorescent Copper Nanoclusters and Their Applications in Cellular Imaging and Catalysis. *Nanoscale* **2014**, *6* (3), 1775−1781.
(16) Rotaru, A.; Dutta, S.; Jentzsch, E.; Gothelf, K.; Mokhir, A. Selective dsDNA-Templated Formation of Copper Nanoparticles in Solution. *Angew. Chem., Int. Ed.* **2010**, *49* (33), 5665−5667.
(17) Jia, X. F.; Li, J.; Han, L.; Ren, J. T.; Yang, X.; Wang, E. DNA-Hosted Copper Nanoclusters for Fluorescent Identification of Single Nucleotide Polymorphisms. *ACS Nano* **2012**, *6* (4), 3311−3317.
(18) Wei, W.; Lu, Y.; Chen, W.; Chen, S. One-Pot Synthesis, Photoluminescence, and Electrocatalytic Properties of Subnanometer-Sized Copper Clusters. *J. Am. Chem. Soc.* **2011**, *133* (7), 2060−2063.
(19) Yang, S.; Sun, S.; Zhou, C.; Hao, G.; Liu, J.; Ramezani, S.; Yu, M.; Sun, X.; Zheng, J. Renal Clearance and Degradation of Glutathione-Coated Copper Nanoparticles. *Bioconjugate Chem.* **2015**, *26* (3), 511−519.
(20) Ma, J. Y.; Chen, P. C.; Chang, H. T. Detection of Hydrogen Sulfide through Photoluminescence Quenching of Penicillamine-Copper Nanocluster Aggregates. *Nanotechnology* **2014**, *25* (19), 195502.
(21) Li, Z.; Guo, S.; Lu, C. A Highly Selective Fluorescent Probe for Sulfide Ions Based on Aggregation of Cu Nanocluster Induced Emission Enhancement. *Analyst* **2015**, *140* (8), 2719−2725.
(22) Nguyen, T. A.; Jones, Z. R.; Goldsmith, B. R.; Buratto, W. R.; Wu, G.; Scott, S. L.; Hayton, T. W. A Cu_{25} Nanocluster with Partial Cu(0) Character. *J. Am. Chem. Soc.* **2015**, *137* (41), 13319−13324.
(23) Jia, X.; Yang, X.; Li, J.; Li, D.; Wang, E. Stable Cu Nanoclusters: From an Aggregation-Induced Emission Mechanism to Biosensing and Catalytic Applications. *Chem. Commun.* **2014**, *50* (2), 237−239.
(24) Kang, X.; Wang, S.; Song, Y.; Jin, S.; Sun, G.; Yu, H.; Zhu, M. Bimetallic Au_2Cu_6 Nanoclusters: Strong Luminescence Induced by the Aggregation of Copper(I) Complexes with Gold(0) Species. *Angew. Chem., Int. Ed.* **2016**, *55* (11), 3611−3614.
(25) Goswami, N.; Yao, Q.; Luo, Z.; Li, J.; Chen, T.; Xie, J. Luminescent Metal Nanoclusters with Aggregation-Induced Emission. *J. Phys. Chem. Lett.* **2016**, *7* (6), 962−975.
(26) Su, X.; Jiang, H.; Wang, X. Thiols-Induced Rapid Photoluminescent Enhancement of Glutathione-Capped Gold Nanoparticles for Intracellular Thiols Imaging Applications. *Anal. Chem.* **2015**, *87* (20), 10230−10236.
(27) Hong, Y. N.; Lam, J. W. Y.; Tang, B. Z. Aggregation-Induced Emission. *Chem. Soc. Rev.* **2011**, *40* (11), 5361−5388.
(28) Liang, J.; Kwok, R. T.; Shi, H.; Tang, B. Z.; Liu, B. Fluorescent Light-up Probe with Aggregation-Induced Emission Characteristics for Alkaline Phosphatase Sensing and Activity Study. *ACS Appl. Mater. Interfaces* **2013**, *5* (17), 8784−8789.
(29) Jia, X.; Li, J.; Wang, E. Cu Nanoclusters with Aggregation Induced Emission Enhancement. *Small* **2013**, *9* (22), 3873−3879.
(30) Wu, Z.; Liu, J.; Gao, Y.; Liu, H.; Li, T.; Zou, H.; Wang, Z.; Zhang, K.; Wang, Y.; Zhang, H.; Yang, B. Assembly-Induced Enhancement of Cu Nanoclusters Luminescence with Mechanochromic Property. *J. Am. Chem. Soc.* **2015**, *137* (40), 12906−12913.
(31) Huang, Y.; Liu, W.; Feng, H.; Ye, Y.; Tang, C.; Ao, H.; Zhao, M.; Chen, G.; Chen, J.; Qian, Z. Luminescent Nanoswitch Based on Organic-Phase Copper Nanoclusters for Sensitive Detection of Trace Amount of Water in Organic Solvents. *Anal. Chem.* **2016**, *88* (14), 7429−7434.
(32) Chen, P. C.; Li, Y. C.; Ma, J. Y.; Huang, J. Y.; Chen, C. F.; Chang, H. T. Size-Tunable Copper Nanocluster Aggregates and Their Application in Hydrogen Sulfide Sensing on Paper-Based Devices. *Sci. Rep.* **2016**, *6*, 24882.
(33) Rieter, W. J.; Pott, K. M.; Taylor, K. M. L.; Lin, W. Nanoscale Coordination Polymers for Platinum-Based Anticancer Drug Delivery. *J. Am. Chem. Soc.* **2008**, *130* (35), 11584−11585.
(34) Zhang, X. D.; Luo, Z. T.; Chen, J.; Shen, X.; Song, S. S.; Sun, Y. M.; Fan, S. J.; Fan, F. Y.; Leong, D. T.; Xie, J. P. Ultrasmall $Au_{10-12}(SG)_{(10-12)}$ Nanomolecules for High Tumor Specificity and Cancer Radiotherapy. *Adv. Mater.* **2014**, *26* (26), 4565−4568.
(35) Shang, L.; Dong, S.; Nienhaus, G. U. Ultra-Small Fluorescent Metal Nanoclusters: Synthesis and Biological Applications. *Nano Today* **2011**, *6* (4), 401−418.
(36) Chen, D.; Zhao, C.; Ye, J.; Li, Q.; Liu, X.; Su, M.; Jiang, H.; Amatore, C.; Selke, M.; Wang, X. In Situ Biosynthesis of Fluorescent Platinum Nanoclusters: Toward Self-Bioimaging-Guided Cancer Theranostics. *ACS Appl. Mater. Interfaces* **2015**, *7* (32), 18163−18169.
(37) Vinluan, R. D., III; Liu, J.; Zhou, C.; Yu, M.; Yang, S.; Kumar, A.; Sun, S.; Dean, A.; Sun, X.; Zheng, J. Glutathione-Coated Luminescent Gold Nanoparticles: A Surface Ligand for Minimizing Serum Protein Adsorption. *ACS Appl. Mater. Interfaces* **2014**, *6* (15), 11829−11833.
(38) Komiya, N.; Muraoka, T.; Iida, M.; Miyanaga, M.; Takahashi, K.; Naota, T. Ultrasound-Induced Emission Enhancement Based on Structure-Dependent Homo- and Heterochiral Aggregations of Chiral Binuclear Platinum Complexes. *J. Am. Chem. Soc.* **2011**, *133* (40), 16054−16061.
(39) Zhou, C.; Sun, C.; Yu, M. X.; Qin, Y. P.; Wang, J. G.; Kim, M.; Zheng, J. Luminescent Gold Nanoparticles with Mixed Valence States Generated from Dissociation of Polymeric Au(I) Thiolates. *J. Phys. Chem. C* **2010**, *114* (17), 7727−7732.
(40) Wang, D.; Li, Y. Controllable Synthesis of Cu-Based Nanocrystals in ODA Solvent. *Chem. Commun.* **2011**, *47* (12), 3604−3606.
(41) Wang, C.; Yao, Y.; Song, Q. Interfacial Synthesis of Polyethyleneimine-Protected Copper Nanoclusters: Size-Dependent Tunable Photoluminescence, pH Sensor and Bioimaging. *Colloids Surf., B* **2016**, *140*, 373−381.
(42) Liu, P.; Hensen, E. J. M. Highly Efficient and Robust Au/$MgCuCr_2O_4$ Catalyst for Gas-Phase Oxidation of Ethanol to Acetaldehyde. *J. Am. Chem. Soc.* **2013**, *135* (38), 14032−14035.
(43) Platzman, I.; Brener, R.; Haick, H.; Tannenbaum, R. Oxidation of Polycrystalline Copper Thin Films at Ambient Conditions. *J. Phys. Chem. C* **2008**, *112* (4), 1101−1108.
(44) Peng, Y.; Shang, L.; Cao, Y. T.; Waterhouse, G. I. N.; Zhou, C.; Bian, T.; Wu, L. Z.; Tung, C. H.; Zhang, T. R. Copper(I) Cysteine Complexes: Efficient Earth-Abundant Oxidation Co-Catalysts for Visible Light-Driven Photocatalytic H_2 Production. *Chem. Commun.* **2015**, *51* (63), 12556−12559.
(45) Wang, F.; Liu, X. Q.; Lu, C. H.; Willner, I. Cysteine-Mediated Aggregation of Au Nanoparticles: The Development of a H_2O_2 Sensor and Oxidase-Based Biosensors. *ACS Nano* **2013**, *7* (8), 7278−7286.
(46) Xiao, Q.; Shang, F.; Xu, X.; Li, Q.; Lu, C.; Lin, J. M. Specific Detection of Cysteine and Homocysteine in Biological Fluids by Tuning the pH Values of Fluorosurfactant-Stabilized Gold Colloidal Solution. *Biosens. Bioelectron.* **2011**, *30* (1), 211−215.
(47) Nam, J.; Won, N.; Jin, H.; Chung, H.; Kim, S. pH-Induced Aggregation of Gold Nanoparticles for Photothermal Cancer Therapy. *J. Am. Chem. Soc.* **2009**, *131* (38), 13639−13645.
(48) Benito, Q.; Baptiste, B.; Polian, A.; Delbes, L.; Martinelli, L.; Gacoin, T.; Boilot, J. P.; Perruchas, S. Pressure Control of Cuprophilic Interactions in a Luminescent Mechanochromic Copper Cluster. *Inorg. Chem.* **2015**, *54* (20), 9821−9825.
(49) Briñas, R. P.; Hu, M.; Qian, L.; Lymar, E. S.; Hainfeld, J. F. Gold Nanoparticle Size Controlled by Polymeric Au(I) Thiolate Precursor Size. *J. Am. Chem. Soc.* **2008**, *130* (3), 975−982.
(50) Vázquezvázquez, C.; Bañobrelópez, M.; Mitra, A.; Lópezquintela, M. A.; Rivas, J. Synthesis of Small Atomic Copper Clusters in Microemulsions. *Langmuir* **2009**, *25* (14), 8208−8216.
(51) Lynch, I.; Dawson, K. A. Protein-Nanoparticle Interactions. *Nano Today* **2008**, *3* (1−2), 40−47.
(52) Liu, J.; Fu, S.; Yuan, B.; Li, Y.; Deng, Z. Toward a Universal "Adhesive Nanosheet" for the Assembly of Multiple Nanoparticles Based on a Protein-Induced Reduction/Decoration of Graphene Oxide. *J. Am. Chem. Soc.* **2010**, *132* (21), 7279−7281.

DOI: 10.1021/acsami.6b13914
ACS Appl. Mater. Interfaces 2017, 9, 3902−3910

(53) Wang, J. Electrochemical Glucose Biosensors. *Chem. Rev.* **2008**, *108* (2), 814−825.
(54) Zhao, Y.; Fan, L.; Zhang, Y.; Zhao, H.; Li, X.; Li, Y.; Wen, L.; Yan, Z.; Huo, Z. Hyper-Branched Cu@Cu_2O Coaxial Nanowires Mesh Electrode for Ultra-Sensitive Glucose Detection. *ACS Appl. Mater. Interfaces* **2015**, *7* (30), 16802−16812.
(55) Liu, M.; Liu, R.; Chen, W. Graphene Wrapped Cu_2O Nanocubes: Non-Enzymatic Electrochemical Sensors for the Detection of Glucose and Hydrogen Peroxide with Enhanced Stability. *Biosens. Bioelectron.* **2013**, *45*, 206−212.

DOI: 10.1021/acsami.6b13914
ACS Appl. Mater. Interfaces 2017, 9, 3902−3910